Magnetic properties of $Ni_{50}Mn_{34.8}In_{15.2}$ probed by Mössbauer spectroscopy

V. V. Khovaylo* and T. Kanomata
Faculty of Engineering, Tohoku Gakuin University, Tagajo 985-8537, Japan

T. Tanaka, M. Nakashima, and Y. Amako
Faculty of Science, Shinshu University, Matsumoto 390-8621, Japan

R. Kainuma, R. Y. Umetsu, and H. Morito
Institute of Multidisciplinary Research for Advanced Materials, Tohoku University, Sendai 980-8577, Japan

H. Miki
Institute of Fluid Science, Tohoku University, Sendai 980–8577, Japan

(Received 27 May 2009; revised manuscript received 23 September 2009; published 14 October 2009)

Structural and magnetic properties of a $Ni_{50}Mn_{34.8}In_{15.2}$ ferromagnetic shape memory alloy doped by ^{57}Fe at the Mn sites have been studied by x-ray diffraction, Mössbauer spectroscopy and superconducting quantum interference device magnetometry. Obtained experimental results have disclosed unique magnetostructural transition from a *high-temperature ferromagnetic austenitic phase* to a *low-temperature paramagnetic martensitic phase* at M_f=290 K. Complex magnetic ordering which can be classified as a cluster glass state is formed in $Ni_{50}Mn_{34.3}$ $^{57}Fe_{0.5}In_{15.2}$ on further cooling below T_C^M=162 K. The abnormal magnetostructural transition observed in $Ni_{50}Mn_{34.3}$ $^{57}Fe_{0.5}In_{15.2}$ is suggested to originate from the weakening of exchange interactions due to an abrupt change in Mn-Mn interatomic distances occurring upon the martensitic transformation.

DOI: 10.1103/PhysRevB.80.144409 PACS number(s): 75.30.Kz, 64.70.kd, 81.30.Kf

I. INTRODUCTION

Materials demonstrating both long-range magnetic ordering and thermoelastic martensitic transformation have attracted growing attention since 1996 when Ullakko *et al.*[1] reported on a giant magnetic field-induced strain in off-stoichiometric Ni_2MnGa Heusler alloy. Since that time, a number of other Heusler-based ferromagnetic shape memory alloys have been discovered. One of the most interesting recent finding has been the observation of structural instability in $Ni_{50}Mn_{25+x}Z_{25-x}$ (Z=In, Sn, Sb).[2] Contrary to Ni_2MnGa-based alloys,[3] a drastic drop of the saturation magnetization has been observed in $Ni_{50}Mn_{25+x}Z_{25-x}$ upon structural transformation from the high-temperature austenitic to the low-temperature martensitic phase.[4–10] Experimental[4–8] and theoretical[11,12] studies have indicated that the enhancement of antiferromagnetic interactions in the martensitic phase is responsible for the observed reduction in the magnetization. In addition to this, some of the $Ni_{50}Mn_{25+x}Z_{25-x}$ alloys have been reported to transform on cooling from the highly magnetized austenitic state to a virtually nonmagnetic martensitic phase.[4,8,13–18] On further cooling, the nonmagnetic martensitic phase transforms to a magnetically ordered state with competing magnetic interactions, as can be judged by the splitting of zero-field-cooling and field-cooling curves and the exchange bias phenomenon;[19–22] the crystal structure of the martensite remains intact.

Transformation from the high-temperature ferromagnetic austenitic phase to the low-temperature martensitic phase with zero net magnetization brings about a number of interesting effects from a practical point of view, such as inverse magnetocaloric effect,[16,23] giant strain due to a field-induced reverse martensitic transformation,[15,24] and giant magnetoresistivity.[25,26] Such effects have been found to accompany the exchange inversion in FeRh,[27–29] Mn_3GaC,[30–32] and CoMnSi (Refs. 33 and 34) intermetallic compounds. This would imply that the ferromagnetic austenitic phase of $Ni_{50}Mn_{25+x}Z_{25-x}$ transforms on cooling to an antiferromagnetic martensite. However, the results of a recent study of $Ni_{50}Mn_{25+x}Sn_{25-x}$ have indicated[35] that a paramagnetic martensitic phase exists in a limited temperature interval below the high-temperature ferromagnetic austenitic phase. In order to shed a light on the magnetism of another representative of ferromagnetic shape memory alloys, $Ni_{50}Mn_{25+x}In_{25-x}$, we undertook superconducting quantum interference device (SQUID) magnetometry and Mössbauer spectroscopy studies of $Ni_{50}Mn_{34.8}In_{15.2}$. The results obtained clearly point to the uncommon sequence of magnetic phase transitions in this alloys, where a paramagnetic phase in sandwiched between two magnetically ordered phases (see Fig. 1).

II. SAMPLE PREPARATION AND MEASUREMENTS

Polycrystalline ingot of a $Ni_{50}Mn_{34.3}$ $^{57}Fe_{0.5}In_{15.2}$ composition doped with 99.5% enriched ^{57}Fe was prepared using a conventional arc-melting method. Since the weight loss after the melting was negligible, the nominal composition was accepted as corresponding to the real one. The ingot was annealed in vacuum at 1173 K for 24 h and quenched in water. Powdered samples prepared from a part of the ingot were used for calorimetric, magnetic, and Mössbauer spectroscopy measurements. Crystal structure was characterized by x-ray diffraction (XRD) using Cu K_α radiation. Characteristic temperatures of the direct and reverse martensitic transformations were determined from differential scanning calorimetry (DSC) measurements performed with a heating/cooling rate 5 K/min. Temperature and field dependencies of the magne-

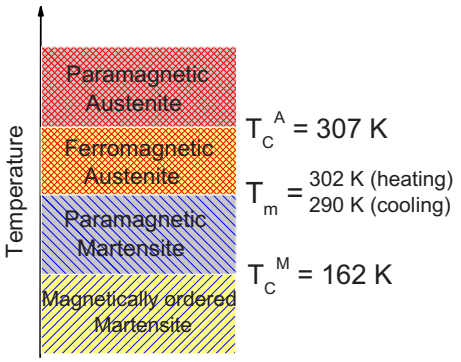

FIG. 1. (Color online) Schematic magnetic phase diagram of the off-stoichiometric $Ni_{50}Mn_{25+x}In_{25-x}$ (x=9.8). T_C^A=307 K is Curie temperature of the austenitic phase, T_m corresponds to the structural transition temperature (austenite start temperature A_s=302 K for the reverse martensitic transformation and martensite finish temperature M_f=290 K for the direct martensitic transformation), and T_C^M=162 K is Curie temperature of the martensitic phase.

tization were measured by a Quantum Design SQUID magnetometer in magnetic fields up to 5 T. ^{57}Fe Mössbauer spectroscopy measurements were carried out in transmission geometry using a conventional spectrometer with a ^{57}Co-Rh source. The obtained spectra were fitted with the help of MOSSWINN 3.0 program.

III. EXPERIMENTAL RESULTS

XRD patterns of $Ni_{50}Mn_{34.3}$ $^{57}Fe_{0.5}In_{15.2}$ measured at room temperature and at T=320 K are depicted in Fig. 2. Cubic symmetry of the high-temperature austenitic phase is evident from the XRD pattern taken at T=320 K [Fig. 2(a)]. Calculated crystal lattice parameter of the $L2_1$ Heusler structure is a=0.5998 nm. The room temperature XRD exhibits complicated pattern as shown in Figs. 2(b) and 2(c). Recently, it has been confirmed by the transmission electronic microscopic observation that a mixture of 10- and 14-layered monoclinic martensitic phases, i.e., the 10M and the 14M phases, appears in NiMnIn and NiCoMnIn alloys.[13,17] Layered structures, such as the 10M- and 14M-type structures [$(3\bar{2})_2$ and $(5\bar{2})_2$ in Zhdanov notation, respectively], are sometimes considered as a tetragonal structure having a high density of ordered nanotwins.[36] If the 10M- and 14M-type structures own the same stacking unit composed of the distorted $L2_1$ phase [denoted as a face-centered tetragonal (fct) structure in Fig. 3], the lattice parameters for the 10M- and 14M-type structures can be easily evaluated on the basis of the 2M structure whose lattice correspondence with the fct structure is as follow: $a_{2M}=c_{2M}=(\sqrt{a_{\mathrm{fct}}^2+c_{\mathrm{fct}}^2})/2$ and $b_{2M}=a_{\mathrm{fct}}$. In the present study, the lattice parameters of the 2M structure, a_{2M}=0.4377 nm, b_{2M}=0.5654 nm, c_{2M}=0.4377 nm, and β_{2M}=99.54°, which correspond to a_{fct}=0.5654 nm and c_{fct}=0.6684 nm for the fct structure, were determined from some reflections, such as $(202)_{\mathrm{fct}}$ [i.e., $(002)_{2M}$ and $(200)_{2M}$] and $(400)_{\mathrm{fct}}$ [i.e., $(040)_{2M}$ and $(202)_{2M}$] at about 2θ=42° and 66°, respectively, that are almost independent of the stacking sequence [Fig. 2(b)]. This result

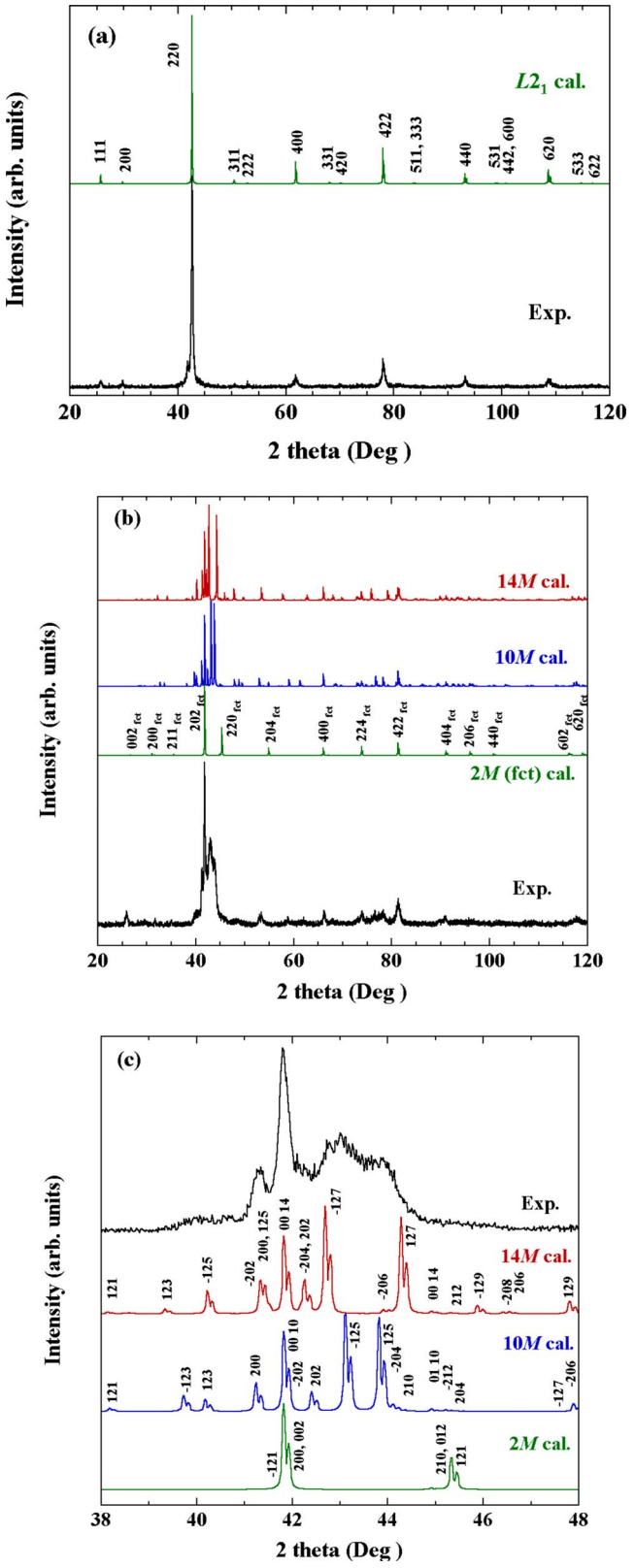

FIG. 2. (Color online) X-ray powder diffraction patterns of $Ni_{50}Mn_{34.3}$ $^{57}Fe_{0.5}In_{15.2}$ measured at T=320 K (a) and at room temperature (b) and (c). Calculated patterns are estimated on the basis of some fundamental lines appearing in the experimental pattern (see text).

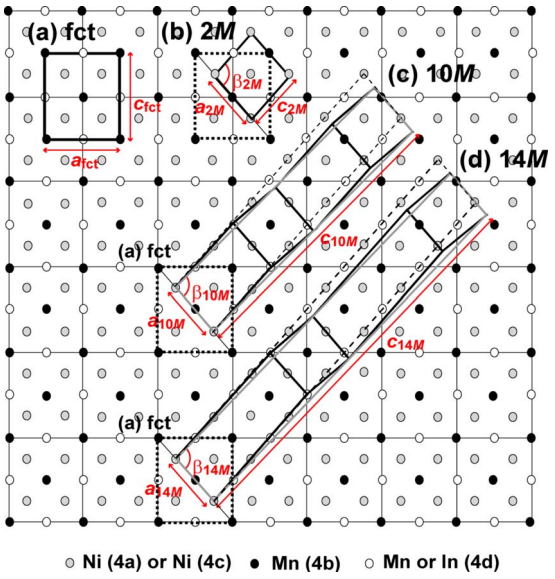

FIG. 3. (Color online) Projections of the face-centered tetragonal (a), 2*M* (b), 10*M* (c), and 14*M* (d) structures on *b* axis.

means that the basic tetragonal distortions from the $L2_1$ phase due to the martensitic transformation are about −6% along *a* axis and about +11% along *c* axis, and that the volume change is about −1%. The monoclinic angle β of the stacking structures can be evaluated as[37]

$$\tan(\beta - 90°) = A \tan(\beta_0 - 90°), \quad (1)$$

where A $[\equiv(n-m)/(n+m)]$ is a parameter indicating the extent of deviation from 90° in the angle β, and β_0 is the monoclinic angle of the 2*M* structure. For the 2*M*, 10*M*, and 14*M* structures this parameter is $A_{2M}=1$, $A_{10M}=0.2$, and $A_{14M}=0.43$, respectively. Using lattice correspondence between 2*M* and fct structures (Fig. 3), lattice parameters for the 10*M*- and 14*M*-type structures can be refined from the lattice parameters of 2*M* structure as $a_{10M}=a_{14M}=a_{2M}$, $b_{10M}=b_{14M}=b_{2M}$, $c_{10M}=5c_{2M}(\sin\beta_0/\sin\beta_{10M})$, and $c_{14M}=7c_{2M}(\sin\beta_0/\sin\beta_{14M})$. The patterns calculated for the 10*M* and 14*M* structures are shown in Figs. 2(b) and 2(c). The experimental pattern can be completely indexed as a mixture of the 10*M* and 14*M* structures with the lattice parameters $a_{10M}=0.4377$ nm, $b_{10M}=0.5654$ nm, $c_{10M}=2.1594$ nm, $\beta_{10M}=91.93°$, and $a_{14M}=0.4377$ nm, $b_{14M}=0.5654$ nm, $c_{14M}=3.0302$ nm, and $\beta_{14M}=94.35°$, respectively.

In the cubic Heusler structure of $Ni_{50}Mn_{25+x}In_{25-x}$ alloys, Ni atoms occupy equivalent 4*a* and 4*c* (in Wyckhoff notation) positions whereas 4*b* positions are occupied by Mn atoms. The 4*d* positions are occupied by Indium atoms and by the excess Mn atoms. In the $L2_1$ cubic structure at $T=320$ K the distances between Ni and Mn at 4*b* [Mn(4*b*)] position, Ni and Mn at 4*d* [Mn(4*d*)] position, and between nearest [Mn(4*b*)-Mn(4*d*)] and next nearest [Mn(4*b*)-Mn(4*b*)] Mn atoms are $l^{cubic}_{Ni\text{-}Mn(4b)}=l^{cubic}_{Ni\text{-}Mn(4d)}=0.2597$ nm, $l^{cubic}_{Mn(4b)\text{-}Mn(4d)}=0.2999$ nm, and $l^{cubic}_{Mn(4b)\text{-}Mn(4b)}=0.4241$ nm, respectively (Table I). Tetragonal distortions of the cubic structure do not affect arrangement of the atoms due to the diffusionless character of the martensitic transformation but considerably modify distances between the atoms. As compared to the austenitic phase, the Ni-Mn(4*d*) and Ni-Mn(4*b*) distances in the martensitic phase simply increase for 0.3%, whereas both $l^{cubic}_{Mn(4b)\text{-}Mn(4d)}$ and $l^{cubic}_{Mn(4b)\text{-}Mn(4b)}$ are split by the structural distortions into two inequivalent distances (see Table I). Estimated from the XRD measurements changes in the interatomic distances accord well with recently reported results of extended x-ray absorption fine structure measurements.[38]

Results of DSC measurements are shown in Fig. 4(a). The well-defined peaks seen on cooling and heating DSC curves correspond to direct and reverse martensitic transformations, respectively. Temperature dependencies of the magnetization $M(T)$ measured in a magnetic field $H=0.05$ T under zero-field-cooling (ZFC) and field-cooling (FC) protocols have a complex character [Fig. 4(b)]. Splitting of the ZFC and FC curves observed at low temperatures is indicative of a nontrivial magnetic ordering with coexisting antiferromagnetic and ferromagnetic interactions. A sharp drop of the magnetization at $T_C^M=162$ K corresponds to the transition into a nonmagnetic state. Note that the magnetic transition occurs far below the martensitic transformation temperature, i.e., within the low-temperature crystallographic modification of the sample. At higher temperatures the magnetization exhibits a small peak upon heating (ZFC curve) and a large one upon cooling (FC curve). Comparison of the $M(T)$ variation along with the DSC data gives ground to conclude that $Ni_{50}Mn_{34.3}$ $^{57}Fe_{0.5}In_{15.2}$ transforms from a nonmagnetic martensite to the ferromagnetic austenite, which exists (on heating) in a narrow temperature interval from the austenite start

TABLE I. Coordination number (*z*) and distances (*l*) between Ni-Mn and Mn-Mn pairs in the high-temperature $L2_1$ ($a=0.5998$ nm) austenitic *A* and the low-temperature fct ($a=0.5654$ nm, $c=0.6684$ nm) martensitic *M* phases of $Ni_{50}Mn_{34.3}$ $^{57}Fe_{0.5}In_{15.2}$.

Pair	l_A (nm)	z_A	l_M (nm)	z_M	$(l_M-l_A)/l_A$ (%)
Ni-Mn(4*b*)	0.2597	4	0.2605	4	0.3
Ni-Mn(4*d*)	0.2597	4	0.2605	4	0.3
Mn(4*b*)-Mn(4*d*)	0.2999	6	0.2827	4	−5.7
			0.3342	2	11.4
Mn(4*b*)-Mn(4*b*)	0.4241	12	0.3998	4	−5.7
			0.4377	8	3.2

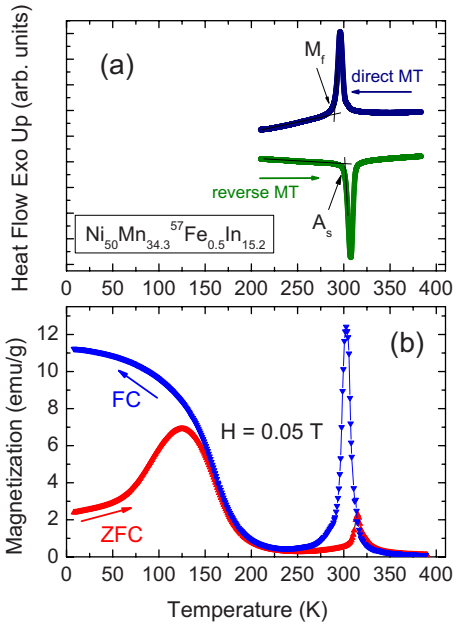

FIG. 4. (Color online) Differential scanning calorimetry (a) and zero-field-cooling (ZFC) and field-cooling (FC) curves (b) of $Ni_{50}Mn_{34.3}{}^{57}Fe_{0.5}In_{15.2}$ alloy. The peaks labeled as "direct MT" and "reverse MT" corresponds to the direct and reverse martensitic transformations, respectively. M_f=290 K is the martensite finish temperature, A_s=302 K is the austenite start temperature. Note that the first-order structural phase transition austenite↔martensite exhibits an intrinsic temperature hysteresis.

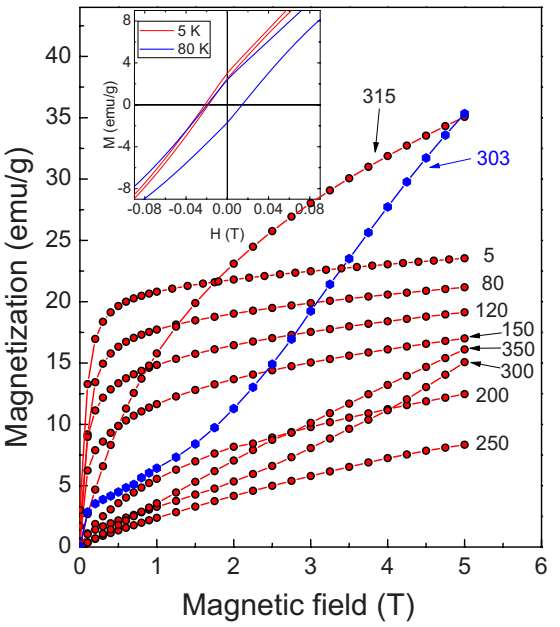

FIG. 5. (Color online) Isothermal magnetization curves of $Ni_{50}Mn_{34.3}{}^{57}Fe_{0.5}In_{15.2}$. The curves were measured while warming the sample, except the curve at T=303 K which was taken at T=303 K after cooling the sample from 352 K. Shown in the inset are low-field parts of the hysteresis loops measured at T=5 K (red curve) and T=80 K (blue curve) in a magnetic field ±5 T.

temperature A_s=302 K to the Curie temperature of the austenite, T_C^A=307 K. On subsequent cooling the direct martensitic transformation occurs at slightly lower temperature than the reverse one [Fig. 4(a)]; hence the feature of the magnetization peak is much more pronounced. Previous works[15,17] have shown that a considerable increase in T_C^A can be attained by a partial substitution of Ni for Co. This makes the ferromagnetic nature of the austenite evident.

Hysteresis loops taken at T=5 and 80 K in a magnetic field ±5 T on the sample field cooled ($H_{cooling}$=2 T) from the paramagnetic austenitic state are shifted from the origin, i.e., exhibit exchange bias (inset in Fig. 5). Since the driving force of exchange bias is a coupling of antiferromagnet and ferromagnet at the interface, this result indicates convincingly that antiferromagnetic and ferromagnetic exchange interactions coexist at low temperatures in the martensitic phase. The observed tendencies of the exchange bias field H_E to decrease from ~200 to ~25 Oe and the coercivity H_C to increase from ~40 to ~350 Oe with increasing temperature are in accordance with earlier reports[19–22] on the exchange bias in $Ni_{50}Mn_{25+x}Z_{25-x}$. The fact that H_E is rather small (~25 Oe) at T=80 K is an indication that this temperature is close to the blocking temperature T_B, above which the uniaxial anisotropy vanishes.

Field dependencies of the magnetization $M(H)$ measured at selected temperatures (Fig. 5) revealed that the magnetization saturation of the martensitic phase gradually decreases with increasing temperature, and at $T \geq 200$ K the response of the low-temperature martensitic phase to the external magnetic field is typical of a paramagnet (or an antiferromagnet). The $M(H)$ curve measured at still higher temperature, T=315 K, where a peak of the ZFC curve is observed [Fig. 4(b)], indicates that even in the vicinity of the Curie temperature T_C^A the magnetization of the austenite is higher than that of the martensite at T=5 K. The distinct feature of the $M(H)$ curve measured in the phase coexistence region (nonmagnetic martensite and ferromagnetic austenite) at T=303 K after cooling the sample from paramagnetic austenitic state is caused by the magnetic field-induced conversion of the nonmagnetic martensite into the ferromagnetic martensite. Thus, the $M(H)$ data (Fig. 5) confirmed results of the $M(T)$ measurements [Fig. 4(b)], which showed that the magnetically ordered low-temperature martensitic and the high-temperature austenitic phases are separated by the martensitic phase with zero net magnetization. It is worth noting that the substitution of Mn by 0.5 at.% ^{57}Fe does not influence the magnetization results. $M(T)$ and $M(H)$ curves measured for $Ni_{50}Mn_{34.8}In_{15.2}$ display the same features as shown in Figs. 4 and 5 for $Ni_{50}Mn_{34.3}{}^{57}Fe_{0.5}In_{15.2}$. Moreover, these data accord well with previously published results[7] for a Ni-Mn-In sample with chemical composition close to that studied in this work.

Since $M(H)$ curves cannot give an unambiguous answer on the magnetic state of the nonmagnetic phase, we probed magnetic properties of the $Ni_{50}Mn_{34.3}{}^{57}Fe_{0.5}In_{15.2}$ sample by ^{57}Fe Mössbauer spectroscopy measurements. The Mössbauer spectra recorded at fixed temperatures from 80 to 352 K while warming the sample are shown in Fig. 6. The spectrum taken at 80 K, i.e., in the magnetically ordered martensitic phase, has a broad sextet arising from a wide distribution of the hyperfine fields. Although there is a good understanding of hyperfine fields in Heusler alloys,[39] the noncubic symme-

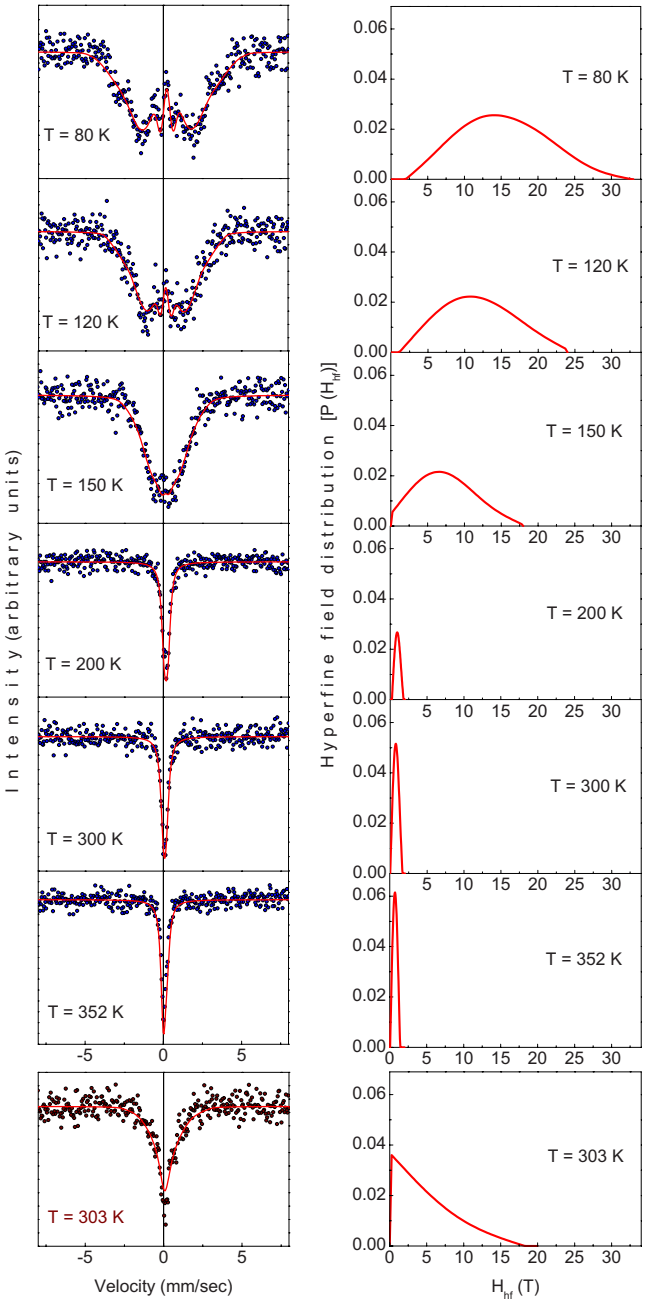

FIG. 6. (Color online) Left panel: experimental (dots) and fitted (solid lines) Mössbauer spectra of $Ni_{50}Mn_{34.3}$ $^{57}Fe_{0.5}In_{15.2}$ recorded at the indicated temperatures while warming the sample. Right panel: corresponding hyperfine field distribution $P(H_{hf})$. Shown in lower panels are Mössbauer spectrum and its hyperfine field distribution measured at $T=303$ K after cooling the sample from 352 K.

try of $Ni_{50}Mn_{34.3}$ $^{57}Fe_{0.5}In_{15.2}$ at 80 K prevented us from qualitative analysis of the spectrum. Moreover, for the off-stoichiometric composition of the sample studied here the excess Mn atoms occupy 4*d* positions, i.e., the In sites. We assume that ^{57}Fe occupy the Mn sites and because of the nonstochiometry ($x=9.8$) of the Heusler alloy some of the ^{57}Fe probe atoms also occupy the In sites. This presumably also influences the Mössbauer spectra shown in Fig. 6.

It is evident from Fig. 6 that the complex Mössbauer absorption spectrum observed at $T=80$ K gradually transforms

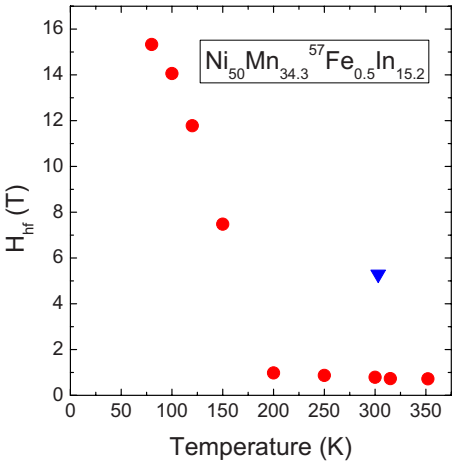

FIG. 7. (Color online) Effective hyperfine field H_{hf} in $Ni_{50}Mn_{34.3}$ $^{57}Fe_{0.5}In_{15.2}$ as a function of temperature. H_{hf} for the sample cooled from 352 K is depicted by the triangle.

to a single-lined one as temperature is increased. The single peak observed on the spectra taken at $T \geq 200$ K excludes scenario of an antiferromagnetic ordering and unambiguously points to paramagnetic properties of the martensite at temperatures above $T_C^M = 162$ K. On the other hand, a sizable contribution from a magnetically ordered phase is seen on the spectrum recorded at 303 K after cooling the sample from 352 K (lower panel of Fig. 6). This is an indication that at this temperature the ferromagnetic high-temperature austenitic phase coexists with the paramagnetic low-temperature martensitic phase.

The hyperfine field distributions obtained from fitting of the spectra are shown in the right panels of Fig. 6. From these fits, the existence of the paramagnetic phase located between two magnetically ordered phases is clearly evident as well. The effective hyperfine field H_{hf} rapidly decreases with increasing temperature and disappears at $T \geq 200$ K (Fig. 7).

IV. DISCUSSION AND CONCLUSION

The observed abnormal magnetic phase transition sequence (magnetically ordered martensite with competing exchange interactions → paramagnetic martensite → ferromagnetic austenite) could be explained as due solely to a strong dependence of the exchange interactions on interatomic distances.[40] Indeed, recent theoretical studies[12,41,42] have shown that the exchange interactions in Mn-based Heusler alloys can be treated in the framework of a Ruderman-Kittel-Kasuya-Yoshida model. However, in $Ni_{50}Mn_{34.3}$ $^{57}Fe_{0.5}In_{15.2}$ two sets of the Mn-Mn distances [i.e., Mn(4*b*)-Mn(4*b*) and Mn(4*b*)-Mn(4*d*)] in the austenitic state are split into four sets in the low-temperature martensitic state due to the structural distortions of the cubic lattice (Table I). Taking into account coordination number, it can be said that the major changes of the exchange interactions originate from the decrease in the Mn(4*b*)-Mn(4*d*) distance and the increase in the Mn(4*b*)-Mn(4*b*) distance. Assuming that the Mn-Mn interaction curve is the same in the austen-

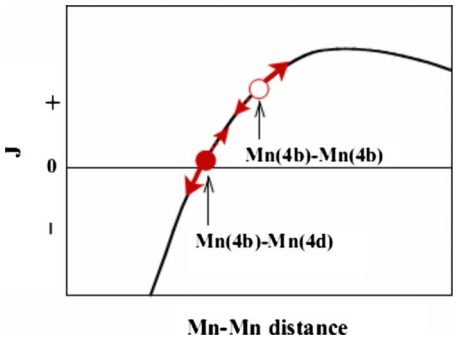

FIG. 8. (Color online) Sketch of Mn-Mn exchange interaction curve in Ni_2MnIn-based Heusler alloys.

itic and the martensitic phase, it can be suggested that at least the larger part of the Mn(4*b*)-Mn(4*d*) interactions are antiferromagnetic in the martensitic phase (Fig. 8). The sign of the rest Mn(4*b*)-Mn(4*d*) interactions and the strength of the Mn(4*b*)-Mn(4*b*) interactions cannot be properly estimated without knowledge of the Mn-Mn interaction curve in the martensitic phase.

Alongside with this, other factors such as changes in the density of states of *sp* electrons and in the *sp-d* mixing caused by the martensitic transformation, has to be considered when discussing abnormal magnetic phase transition sequence in the studied alloy. Importance of these factors in establishing magnetic properties and the type of magnetic order has been noticed both experimentally[43] and theoretically.[42]

Considering magnetic properties of the martensitic phase at temperatures below $T_C^M = 162$ K, magnetic heterogeneity of $Ni_{50}Mn_{34.3}$ $^{57}Fe_{0.5}In_{15.2}$ is evident from the observation of exchange bias (inset in Fig. 5). Since total magnetic moment in this alloy is largely confined to the Mn atoms, it is very likely that the antiferromagnetism leading to the interface exchange coupling is dominated by the Mn(4*b*)-Mn(4*d*) interaction; the Ni-Mn(4*d*) [Ni-Mn(4*b*)] interactions give small if any contribution. A circumstantial evidence for this suggestion is a small net magnetic moment of the martensitic phase which is equal to $\sim 1 \mu_B$ at 5 K in the studied alloy (Fig. 5). Since the distribution of Mn atoms in the In sublattice is evidently random, it is natural to assume that antiferromagnetically ordered clusters are formed within ferromagnetically ordered matrix. In this sense the low-temperature magnetic phase should be considered as a cluster glass. This is somewhat similar to magnetic properties of hole-doped manganites where intrinsic interface exchange coupling is realized due to phase separation.[44]

In conclusion, the most important finding of our Mössbauer spectroscopy studies is that the low-temperature martensitic phase of $Ni_{50}Mn_{34.3}$ $^{57}Fe_{0.5}In_{15.2}$ is *paramagnetic* at temperatures above $T_C^M = 162$ K. To the best our knowledge, $Ni_{50}Mn_{25+x}Z_{25-x}$ (Z=In, Sn) ferromagnetic shape memory alloys are the only ones representing unique magnetostructural phase transitions from the *low-temperature paramagnetic* to the *high-temperature ferromagnetic phase*. The uncommon phase transition sequence is suggested to originate from the weakening of exchange interactions due to an abrupt change of the Mn-Mn interatomic distances occurring upon the martensitic transformation.

ACKNOWLEDGMENTS

This work was partially supported by the Russian Foundation for Basic Research (Grants No. 06-02-39030 and No. 08-02-91317), by a Grant-in-Aid for Scientific Research from the Japan Society for the Promotion of Science, by Japan Science and Technology Agency and by a grant based on the High-Tech Research Center Program for private universities from the Japan Ministry of Education, Culture, Sports, Science and Technology.

*Present address: National University of Science and Technology "Moscow Institute of Steel and Alloys," Moscow 119049, Russia.

[1] K. Ullakko, J. K. Huang, C. Kantner, R. C. O'Handley, and V. V. Kokorin, Appl. Phys. Lett. **69**, 1966 (1996).
[2] Y. Sutou, Y. Imano, N. Koeda, T. Omori, R. Kainuma, K. Ishida, and K. Oikawa, Appl. Phys. Lett. **85**, 4358 (2004).
[3] P. J. Webster, K. R. A. Ziebeck, S. L. Town, and M. S. Peak, Philos. Mag. B **49**, 295 (1984).
[4] T. Krenke, M. Acet, E. F. Wassermann, X. Moya, L. Mañosa, and A. Planes, Phys. Rev. B **72**, 014412 (2005).
[5] P. J. Brown, A. P. Gandy, K. Ishida, R. Kainuma, T. Kanomata, K.-U. Neumann, K. Oikawa, B. Ouladdiaf, and K. R. A. Ziebeck, J. Phys.: Condens. Matter **18**, 2249 (2006).
[6] T. Kanomata, K. Fukushima, H. Nishihara, R. Kainuma, W. Itoh, K. Oikawa, K. Ishida, K. U. Neumann, and K. R. A. Ziebeck, Mater. Sci. Forum **583**, 119 (2008).
[7] P. A. Bhobe, K. R. Priolkar, and A. K. Nigam, Appl. Phys. Lett. **91**, 242503 (2007).
[8] M. Khan, I. Dubenko, S. Stadler, and N. Ali, J. Phys.: Condens. Matter **20**, 235204 (2008).
[9] T. Krenke, M. Acet, E. F. Wassermann, X. Moya, L. Mañosa, and A. Planes, Phys. Rev. B **73**, 174413 (2006).
[10] S. Y. Yu, L. Ma, G. D. Liu, Z. H. Liu, J. L. Chen, Z. X. Cao, G. H. Wu, B. Zhang, and X. X. Zhang, Appl. Phys. Lett. **90**, 242501 (2007).
[11] V. D. Buchelnikov, S. V. Taskaev, M. A. Zagrebin, V. V. Khovailo, and P. Entel, J. Magn. Magn. Mater. **320**, E175 (2008).
[12] V. D. Buchelnikov, P. Entel, S. V. Taskaev, V. V. Sokolovsky, A. Hucht, M. Ogura, H. Akai, M. E. Gruner, and S. K. Nayak, Phys. Rev. B **78**, 184427 (2008).
[13] K. Oikawa, W. Ito, Y. Imano, Y. Sutou, R. Kainuma, K. Ishida, S. Okamoto, O. Kitakami, and T. Kanomata, Appl. Phys. Lett. **88**, 122507 (2006).
[14] R. Kainuma, Y. Imano, W. Ito, H. Morito, Y. Sutou, K. Oikawa, A. Fujita, K. Ishida, S. Okamoto, O. Kitakami, and T. Kanomata, Appl. Phys. Lett. **88**, 192513 (2006).
[15] R. Kainuma, Y. Imano, W. Ito, Y. Sutou, H. Morito, S. Okamoto, O. Kitakami, K. Oikawa, A. Fujita, T. Kanomata, and K. Ishida, Nature (London) **439**, 957 (2006).

[16] Z. D. Han, D. H. Wang, C. L. Zhang, S. L. Tang, B. X. Gu, and Y. W. Du, Appl. Phys. Lett. **89**, 182507 (2006).
[17] W. Ito, Y. Imano, R. Kainuma, Y. Sutou, K. Oikawa, and K. Ishida, Metall. Mater. Trans. A **38**, 759 (2007).
[18] W. Ito, M. Nagasako, R. Y. Umetsu, R. Kainuma, T. Kanomata, and K. Ishida, Appl. Phys. Lett. **93**, 232503 (2008).
[19] M. Khan, I. Dubenko, S. Stadler, and N. Ali, Appl. Phys. Lett. **91**, 072510 (2007).
[20] Z. Li, C. Jing, J. Chen, S. Yuan, S. Cao, and J. Zhang, Appl. Phys. Lett. **91**, 112505 (2007).
[21] B. M. Wang, Y. Liu, L. Wang, S. L. Huang, Y. Zhao, Y. Yang, and H. Zhang, J. Appl. Phys. **104**, 043916 (2008).
[22] A. K. Pathak, M. Khan, B. R. Gautam, S. Stadler, I. Dubenko, and N. Ali, J. Magn. Magn. Mater. **321**, 963 (2009).
[23] T. Krenke, E. Duman, M. Acet, E. F. Wassermann, X. Moya, L. Mañosa, and A. Planes, Nature Mater. **4**, 450 (2005).
[24] K. Koyama, K. Watanabe, T. Kanomata, R. Kainuma, K. Oikawa, and K. Ishida, Appl. Phys. Lett. **88**, 132505 (2006).
[25] K. Koyama, H. Okada, K. Watanabe, T. Kanomata, R. Kainuma, W. Ito, K. Oikawa, and K. Ishida, Appl. Phys. Lett. **89**, 182510 (2006).
[26] S. Y. Yu, Z. H. Liu, G. D. Liu, J. L. Chen, Z. X. Cao, G. H. Wu, B. Zhang, and X. X. Zhang, Appl. Phys. Lett. **89**, 162503 (2006).
[27] M. R. Ibarra and P. A. Algarabel, Phys. Rev. B **50**, 4196 (1994).
[28] P. A. Algarabel, M. R. Ibarra, C. Marquina, A. del Moral, J. Galibert, M. Iqbal, and S. Askenazy, Appl. Phys. Lett. **66**, 3061 (1995).
[29] M. P. Annaorazov, S. A. Nikitin, A. L. Tyurin, K. A. Asatryan, and A. Kh. Dovletov, J. Appl. Phys. **79**, 1689 (1996).
[30] K. Kamishima, M. I. Bartashevich, T. Goto, M. Kikuchi, and T. Kanomata, J. Phys. Soc. Jpn. **67**, 1748 (1998).
[31] K. Kamishima, T. Goto, H. Nakagawa, N. Miura, M. Ohashi, N. Mori, T. Sasaki, and T. Kanomata, Phys. Rev. B **63**, 024426 (2000).
[32] M.-H. Yu, L. H. Lewis, and A. R. Moodenbaugh, J. Appl. Phys. **93**, 10128 (2003).
[33] H. Bińczycka, A. Szytuła, J. Todorović, T. Zaleski, and A. Zięba, Phys. Status Solidi A **35**, K69 (1976).
[34] K. G. Sandeman, R. Daou, S. Özcan, J. H. Durrell, N. D. Mathur, and D. J. Fray, Phys. Rev. B **74**, 224436 (2006).
[35] R. Y. Umetsu, R. Kainuma, Y. Amako, Y. Taniguchi, T. Kanomata, K. Fukushima, A. Fujita, K. Oikawa, and K. Ishida, Appl. Phys. Lett. **93**, 042509 (2008).
[36] A. G. Khachaturyan, S. M. Shapiro, and S. Semenovskaya, Phys. Rev. B **43**, 10832 (1991).
[37] R. Kainuma, F. Gejima, Y. Sutou, I. Ohnuma, and K. Ishida, Mater. Trans., JIM **41**, 943 (2000).
[38] P. A. Bhobe, K. R. Priolkar, and P. R. Salode, J. Phys. D **41**, 045004 (2008).
[39] C. C. M. Campbell, T. Birchall, and J. C. Suits, J. Phys. F: Met. Phys. **7**, 727 (1977).
[40] T. Kanomata, T. Yasuda, S. Sasaki, H. Nishihara, R. Kainuma, W. Ito, K. Oikawa, K. Ishida, K.-U. Neumann, and K. R. A. Ziebeck, J. Magn. Magn. Mater. **321**, 773 (2009).
[41] E. Şaşıoğlu, L. M. Sandratskii, and P. Bruno, Phys. Rev. B **70**, 024427 (2004).
[42] E. Şaşıoğlu, L. M. Sandratskii, and P. Bruno, Phys. Rev. B **77**, 064417 (2008).
[43] P. J. Webster and M. R. I. Ramadan, J. Magn. Magn. Mater. **5**, 51 (1977).
[44] D. Niebieskikwiat and M. B. Salamon, Phys. Rev. B **72**, 174422 (2005).